Chem. Mater. **2005,** *17,* 4023−4030

Solubility-Controlled Synthesis of High-Quality Co_3O_4 Nanocrystals

Tao He, Dairong Chen,* Xiuling Jiao, Yingling Wang, and Yongzheng Duan

Department of Chemistry, Shandong University, Jinan 250100, People's Republic of China

Received April 5, 2005. Revised Manuscript Received May 21, 2005

A liquid-phase redox process has been designed to prepare monodispersed Co_3O_4 nanocrystals with particle sizes of 2 nm (spherical), 2.5 nm (cubelike), and 4.7 nm (cubelike). The nanocrystals were characterized by transmission electron microscopy (TEM), high-resolution TEM, X-ray diffraction, X-ray photoelectron spectroscopy, Fourier transform infrared spectroscopy, and thermogravimetric techniques. The nucleation and growth, which were tracked by UV−visible spectroscopy, can be separated by adjusting the solubility of sodium nitrate, and the smallest possible Co_3O_4 nanocubes, 2.5 nm on a side, were obtained. A solubility-controlled mechanism for the redox reaction is discussed which is critical in avoiding secondary nucleation and interparticle ripening growth of Co_3O_4 nanocrystals.

1. Introduction

The uniformity of particle size and shape of nanocrystals is necessary for them to possess desirable physical and chemical properties.[1] The controlled synthesis of nanocrystals with a single size and shape is also important for constructing nanostructured materials by bottom-to-top techniques.[2] Liquid-phase synthesis is a good approach for preparation of inorganic nanoparticles because of the following advantages. First, it allows separation of nucleation and growth which guarantees a narrow particle size distribution. Second, particle size control is also achieved by coating the nuclei surfaces with surfactant molecules to reduce the growth rate or cooling the reaction system to quench growth at a certain particle size. The surfactant coating prevents the nuclei from aggregating.[3] Of all the liquid-phase routes, rapid-injection syntheses have been most intensively used to prepare nanocrystals of metals, semiconductors, and metal oxides with controlled particle size and shape. To obtain a separation of nucleation and grain growth, a fast thermodecomposition of an organometallic precursor in a hot inert organic solvent is induced by rapid injection.[4] Besides rapid-injection syntheses, automatic separation of nucleation and growth in a one-pot liquid-phase process has also been achieved during the formation of CdS nanocrystals by adding a nucleation initiator.[5]

Although great successes have been achieved in liquid-phase processes, the synthesis of nanocrystals with controlled particle size and shape still remains a challenge. In all of the above liquid-phase processes, the inevitable change of reactant concentration over time complicates the nucleation and growth. The excessively high degree of supersaturation of product monomer caused by the large reactant concentration in the initial stage of reaction causes the nuclei to grow very rapidly. Defocusing of particle size distribution caused by Ostwald ripening will occur when the monomer concentration is below the saturation concentration of the smallest particles.[6]

As an important functional material, the p-type semiconductor Co_3O_4 is used in heterogeneous catalysts, anode materials in Li ion rechargeable batteries, solid-state sensors, electrochromic devices, solar energy absorbers, pigments, and other applications.[7] The preparation of the spinel oxide with various nanostructures and their corresponding electric,

---

* Corresponding author. E-mail: cdr@sdu.edu.cn. Fax: +86-0531-8364281.

(1) See, for example: Alivisatos, A. P. *J. Phys. Chem.* **1996**, *100*, 13226.

(2) See, for example: (a) Markovich, G.; Collier, C. P.; Henrichs, S. E.; Remacle, F.; Levine, R. D.; Heath, J. R. *Acc. Chem. Res.* **1999**, *32*, 415. (b) Wang, Z. L.; Harfenist, S. A.; Whetten, R. L.; Bentley, J.; Evans, N. D. *J. Phys. Chem. B* **1998**, *102*, 3068. (c) Böker, A.; Lin, Y.; Chiapperini, K.; Horowitz, R.; Thompson, M.; Carreon, V.; Xu, T.; Abetz, C.; Skaff, H.; Dinsmore, A. D.; Emrick, T.; Russell, T. P. *Nature Mater.* **2004**, *3*, 302. (d) Sun, S.; Murray, C. B.; Weller, D.; Folks, L.; Moser, A. *Science* **2000**, *287*, 1989. (e) Pileni, M. P. *J. Phys. Chem. B* **2001**, *105*, 3358.

(3) Cushing, B. L.; Kolesnichenko, V. L.; O'Connor, C. J. *Chem. Rev.* **2004**, *104*, 3893.

(4) (a) Katari, J. E. B.; Colvin, V. L.; Alivisatos, A. P. *J. Phys. Chem.* **1994**, *98*, 4109. (b) Park, S. J.; Kim, S.; Lee, S.; Khim, Z. G.; Char, K.; Hyeon, T. *J. Am. Chem. Soc.* **2000**, *122*, 8581. (c) Murray, C. B.; Norris, D. J.; Bawendi, M. G. *J. Am. Chem. Soc.* **1993**, *115*, 8706. (d) Cao, Y.; Banin, U. *J. Am. Chem. Soc.* **2000**, *122*, 9692. (e) Steckel, J. S.; Zimmer, J. P.; Coe-Sullivan, S.; Stott, N. E.; Bulovic, V.; Bawendi, M. G. *Angew. Chem., Int. Ed.* **2004**, *43*, 2154. (f) Hines, M. A.; Scholes, G. D. *Adv. Mater.* **2003**, *15*, 1844. (g) Jun, Y. W.; Koo, J. E.; Cheon, J. *Chem. Commun.* **2000**, 1243. (h) Peng, Z. A.; Peng, X. *J. Am. Chem. Soc.* **2002**, *124*, 3343. (i) Rockenberger, J.; Scher, E. C.; Alivisatos, A. P. *J. Am. Chem. Soc.* **1999**, *121*, 11595. (j) Hyeon, T. *Chem. Commun.* **2003**, 927. (k) Trentler, T. J.; Denler, T. E.; Bertone, J. F.; Agrawal, A.; Colvin, V. L. *J. Am. Chem. Soc.* **1999**, *121*, 1613. (l) Cozzoli, P. D.; Curri, M. L.; Agostiano, A. *J. Phys. Chem. B* **2003**, *107*, 4756.

(5) Cao, Y. C.; Wang, J. *J. Am. Chem. Soc.* **2004**, *126*, 14336.

(6) Peng, X.; Wickham, J.; Alivisatos, A. P. *J. Am. Chem. Soc.* **1998**, *120*, 5343.

(7) (a) Busca, G.; Trifirò, F.; Vaccari, A. *Langmuir* **1990**, *6*, 1440. (b) Stavart, A.; Lierde, A. V. *J. Appl. Electrochem.* **2001**, *31*, 469. (c) Poizot, P.; Laruelle, S.; Grugeon, S.; Dupont, L.; Tarascon, J. M. *Nature* **2000**, *407*, 496. (d) Yuan, Z.; Huang, F.; Feng, C.; Sun, J.; Zhou, Y. *Mater. Chem. Phys.* **2003**, *79*, 1. (e) Yamaura, H.; Tamaki, J.; Moriya, K.; Miura, N.; Yamazoe, N. *J. Electrochem. Soc.* **1997**, *144*, L158. (f) Ando, M.; Kobayashi, T.; Lijima, S.; Haruta, M. *J. Mater. Chem.* **1997**, *7*, 1779. (g) Svegl, F.; Orel, B.; Hutchins, M. G.; Kalcher, K. *J. Electrochem. Soc.* **1996**, *143*, 1532. (h) Maruyama, T.; Arai, S. *J. Electrochem. Soc.* **1996**, *143*, 1383. (i) Hutchins, M. G.; Wright, P. J.; Grebenik, P. D. *Solar Energy Mater.* **1987**, *16*, 113. (j) Ramachandram, K.; Oriakhi, C. O.; Lerner, M. M.; Koch, V. R. *Mater. Res. Bull.* **1996**, *31*, 767. (k) Sugimoto, T.; Matijevi'c, E. *J. Inorg. Nucl. Chem.* **1979**, *41*, 165.

10.1021/cm050727s CCC: $30.25

magnetic and catalytic properties have been studied.[8] In early 1978, monodispersed 100-nm Co_3O_4 nanocubes were prepared by means of a traditional forced hydrolysis method.[7k] Spinel oxide cubes with a dimensional scale of ∼10−100 nm were obtained through a salt-mediated preparation process, in which the size and shape control was attributed to a salt-(solvent)n diffusion boundary coating the surfaces of the resulting Co_3O_4 nanoparticles.[8c] Recently, Xu and Zeng have synthesized Co_3O_4 nanocubes smaller than 10 nm and their superstructures by adding capping agent Tween-85 into their reaction system.[8d]

Herein, we describe a liquid-phase redox reaction that generates high-quality Co_3O_4 nanocrystals. It is based on a new synthetic strategy: the oxidation of the reducing species (Co(II)) to form Co_3O_4 in solution was controlled by adjusting the solubility of the oxidizing species (NO_3^-). When the solubility of the oxidant is intentionally limited to an appropriate value, the separation of nucleation and growth of nanocrystals is achieved, and Ostwald ripening is avoided. The strategy is depicted as follows. Cobalt nitrate ($Co(NO_3)_2{\cdot}4H_2O$ or $Co(NO_3)_2{\cdot}7C_6H_{13}OH$) and sodium dodecyl benzenesulfonate (SDBS) are dissolved in *n*-octanol, and a metathesis reaction takes place between them, precipitating sodium nitrate. When a polar solvent such as water, dimethyl sulfoxide (DMSO), or methanol is added into the *n*-octanol solution, the sodium nitrate is redissolved, and thus the solubility of sodium nitrate can be controlled by adjusting the content of water, DMSO or methanol in the system. At higher temperatures, a redox reaction between the reducing species, including Co(II), and the nitrate anions occurs. The thermodynamics and kinetics of the redox reaction as well as the nucleation and growth of nanocrystals are controllable by adjusting the concentration of nitrate anions in solution.

In the solubility-controlled synthesis, the particle size control in the initial stage of growth has been achieved and Co_3O_4 nanocubes with a particle sizes from 2 to 5 nm have been prepared. Their particle size distributions are narrow enough for the resulting particles to form two- and three-dimensional superlattices spontaneously. Moreover, the critical size for a Co_3O_4 particle able to have a cubelike shape is 2.5 nm.

2. Experimental Section

2.1.1. Chemicals. SDBS (>90 wt %, Shanghai Chemical Co.) was kept for use in a glass desiccator, and DMSO (analytically pure, Tianjin Reagent Co.) and *n*-octanol (analytically pure, Tianjin Reagent Co.) were dried over 4-Å molecular sieves. $Co(NO_3)_2{\cdot}7C_6H_{13}OH$ was prepared based on reference.[8j] $Co(NO_3)_2{\cdot}6H_2O$ (analytically pure, Shanghai Chemical Co.) was kept in a glass desiccator using 4-Å molecular sieves as desiccant at room temperature for 3 days to give the compound $Co(NO_3)_2{\cdot}4H_2O$.

Table 1. Reaction Parameters for Different Designed Experiments

exp no.	cobalt source	reaction process
1	$Co(NO_3)_2{\cdot}7C_6H_{13}OH$	90 °C for 6 h
2	$Co(NO_3)_2{\cdot}4H_2O$	90 °C for 6 h
3	$Co(NO_3)_2{\cdot}7C_6H_{13}OH$	90 °C for 6 h, then 180 °C for 6 h
4	$Co(NO_3)_2{\cdot}7C_6H_{13}OH$	90 °C for 6 h, added 0.50 mL of DMSO, then 180 °C for 1.5 h
5	$Co(NO_3)_2{\cdot}7C_6H_{13}OH$	90 °C for 6 h, added 2.00 mL of methanol, then 180 °C for 1.5 h
6	$Co(NO_3)_2{\cdot}4H_2O$	90 °C for 6 h, removed the precipitated sodium nitrate, then 180 °C for 6 h

2.1.2. Typical Synthesis of Co_3O_4 Nanocrystals. $Co(NO_3)_2{\cdot}4H_2O$ (3.44 mmol, 0.8770 g) was dissolved in 22.0 mL *n*-octanol to form a red solution, and then 8.58 mmol (3.3000 g) SDBS was added into the solution under magnetic stirring for 5 min, resulting in a brown solution. The obtained solution was heated at 90 °C for 6 h in a 25-mL autoclave with a Teflon liner and then transferred into an 180 °C oven for a designated time. After that, the autoclave was allowed to cool to room temperature. The 20-mL black liquid was extracted with a mixture of 15 mL of cyclohexane, 10 mL of absolute ethanol, and 25 mL of deionized water. After the water phase was discarded, another 10 mL of absolute ethanol and 25 mL of deionized water was added to the oil phase. The extraction was repeated three or more times, till the oil phase about 15 mL was a transparent deep brown color. A drop of oil phase was placed on the transmission electron microscopy (TEM) grid and used directly for TEM and high-resolution TEM (HRTEM) characterization, and no size sorting was applied when the electron microscope images were obtained. When 15 mL of methanol was added to the oil phase, a black powder precipitate was obtained. The black powder was separated by centrifugation at 6000 rpm for 10 minutes, washed with methanol for three times, and then dried at 100 °C for 1 h. The dried material was used for X-ray photoelectron spectroscopy (XPS), X-ray diffraction (XRD), Fourier-transform infrared (FTIR), and thermogravimetric (TG) characterizations. All the above manipulations were carried out in air with humidity of ca. ∼30−40%.

2.1.3. Testing the Solubility-Controlled Mechanism. To verify that the redox reaction is controlled by the solubility of sodium nitrate, several experiments were carried out as listed in Table 1. Unless otherwise indicated, the amounts of raw material and solvent were the same as in the typical experiment (2.1.2).

2.2. Characterization. 2.2.1. Tracking the Reaction. The phases of the intermediates, separated by centrifugation and without washing or drying, were identified using XRD (scan rate, 1°/min; scan step, 0.02°) on a Rigaku D/Max 2200-PC diffractometer with Cu Kα radiation ($\lambda = 0.15418$ nm) and graphite monochromator at ambient temperature. The components in the reaction solution were identified using UV−visible spectroscopy scanning from 900 to 200 nm (Lambda-35, UV−vis spectrometer, Perkin-Elmer).

2.2.2. Characterization of the As-Prepared Nanocrystals. The particle size distribution, dispersibility, and shape of the prepared nanocrystals were characterized by TEM (JEM100-CXII); the structure and growth of the nanocrystals was observed with HRTEM (GEOL-2010). The strongest peak (311) of the XRD patterns was used to estimate the average size of Co_3O_4 nanocrystals based on the Debye−Scherrer formula. The aggregation-induced superstructures of 2-nm nanocrystals were detected with low-angle XRD at a scanning rate of 1°/min. IR spectra analyses (Nicolet 5DX FT-IR instrument, KBr pellet technique), TG (air flow rate 20 mL/

---

(8) (a) Wang, Y.; Fu, Z. W.; Qin, Q. Z. *Thin Solid Films* **2003**, *441*, 19. (b) Xu, R.; Zeng, H. C. *J. Phys. Chem. B* **2003**, *107*, 12643. (c) Feng, J.; Zeng, H. C. *Chem. Mater.* **2003**, *15*, 2829. (d) Xu, R.; Zeng, H. C. *Langmuir* **2004**, *20*, 9780. (e) Jana, N. R.; Chen, Y.; Peng, X. *Chem. Mater.* **2004**, *16*, 3931. (f) Verelst, M.; Ely, T. O.; Amiens, C.; Snoeck, E.; Lecante, P.; Mosset, A.; Respaud, M.; Broto, J. M.; Chaudret, B. *Chem. Mater.* **1999**, *11*, 2702. (g) Yuan, Z.; Huang, F.; Feng, C.; Sun, J.; Zhou, Y. *Mater. Chem. Phys.* **2003**, *79*, 1. (h) Potoczna, D.; Kępiński, L. *Catal. Lett.* **2001**, *73*, 41. (i) Takada, S.; Fujii, M.; Kohiki, S. *Nano Lett.* **2001**, *1*, 379. (j) He, T.; Chen, D.; Jiao, X. *Chem. Mater.* **2004**, *16*, 737. (k) He, T.; Chen, D.; Jiao, X.; Xu, Y.; Gu, Y. *Langmiur* **2004**, *20*, 8404. (l) Barreca, D.; Massignan, C. *Chem. Mater.* **2001**, *13*, 588. (m) Shi, X. S.; Han, S.; Sanedrin, R. J.; Zhou, F.; Selke, M. *Chem. Mater.* **2002**, *14*, 1897. (n) Lakshmi, B. B.; Patrissi, C. J.; Martin, C. R. *Chem. Mater.* **1997**, *9*, 2544. (o) Liu, Y.; Wang, G.; Xu, C.; Wang, W. *Chem. Commun.* **2002**, 1486.

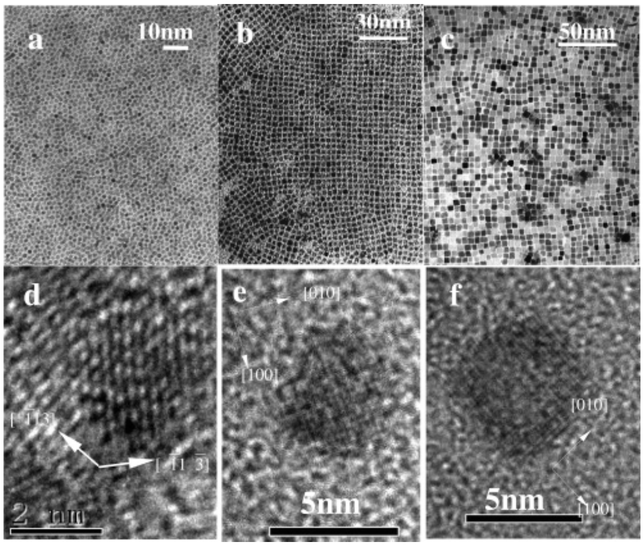

Figure 1. TEM and HRTEM images of Co_3O_4 nanocrystals obtained in the typical synthesis at 180 °C for 1.5 h (a and d 2 -m nanocrystals), 2 h (b and e, 2.5-nm nanocrystals), and 2.5 h (c and f, 4.7-nm nanocrystals).

min, heating rate 10 °C/min), and XPS investigations were applied to characterize the nanocrystals' surface. The XPS spectra were recorded on a PHI-5300 ESCA spectrometer (Perkin-Elmer) with its energy analyzer working in the pass energy mode at 35.75 eV, and the Al Kα line was used as excitation source. The binding energy reference was taken at 284.7 eV for the C1s peak arising from surface hydrocarbons.[9] After subtraction of X-ray satellites and inelastic background (Shirley-type), the peak deconvolution was carried out. Full width at half maximum (fwhm) was kept the same for chemical components within the same core level of an element, and all component peaks were set to be Gaussian-type.

3. Results and Discussion

3.1. Particulate Properties of Co_3O_4 Nanocrystals. The TEM images of Co_3O_4 nanoparticles produced by the typical synthesis are shown in Figure 1. The resulting Co_3O_4 nanoparticles are monodispersed, and the average particle sizes are 2.0 nm (standard deviation 9%), 2.5 nm (standard deviation 10%), and 4.7 nm (standard deviation 10%), respectively. The 2-nm particles are roughly spherical, while the larger particles are all nanocubes. The lattice fringes in the HRTEM images reveal their single-crystal nature. The lattice plane distances of 0.244 nm ($\bar{1}1\bar{3}$) and 0.244 nm ($\bar{1}13$), as well as the angle of ca. 130° between the crossed fringes, indicate that the exhibited facet of the 2-nm nanocrystal in HRTEM images is (110) lattice plane of the spinel oxide. On the other hand, all the four-square facets of the nanocubes are {100} lattice planes, which is consistent with the fact that {100} lattice planes of *fcc* are of 4-fold symmetry (JCPDS file, No. 43-1003). Each kind of particle arranges spontaneously to form a two-dimensional closed packed structure on the TEM grid, demonstrating the uniformity of the particle size. Moreover, the 2-nm spherical particles form a two-dimensional hexagonally closed packed array and the other nanocubes are squarely packed, which results from the shape effect of the nanocrystals on self-assembly.[8d,10] The interparticle intervals in the two-dimensional arrays of 2- and 2.5-nm nanocrystals are always 1.8 nm, indicating that the same capping molecules exist on their surfaces.

The XRD patterns (Figure 2a) show that all the products are pure spinel oxide Co_3O_4. The intense broadening of the peaks is caused by the quite small particle sizes, and the broad peak at 20° is mainly caused by the diffraction of glass. The calculated particle sizes based on the Debye−Scherrer formula are 1.9, 2.5, and 4.6 nm, respectively, roughly consistent with the statistical values from the TEM images.[11] The precipitated powders can be redissolved in hydrocarbons (such as cyclohexane, liquid paraffin, and long-carbon-chain alcohols) to form a transparent solution. The good dispersibility was not destroyed even when the powders were heated in a vacuum at 120 °C for 2.5 h. A peak at ca. 1.5° appears in the low-angle XRD patterns (Figure 2b), indicating the formation of nanocrystal superlattices during precipitation, which further confirms the uniform particle sizes of nanocrystals. Moreover, the 2-nm crystals self-assemble into superstructured hollow spheres if precipitation is induced with a solution of methanol and deionized water (Supporting Information, Figure S1). The formation mechanism of these superstructures needs further investigation.

3.2. Particle Surface of Co_3O_4 Nanocrystals. The rapid weight losses from 180 to 280 °C in TG curves resulted from the elimination of adsorbed alcohol molecules (mainly *n*-octanol molecules) on the nanocrystals' surfaces (Figure 3a).[8j] The weight loss centered at ca. 300 °C is attributed to the elimination of chemically adsorbed carboxylate anions probably originating from the oxidation of *n*-octanol during the synthetic process (see below). From 700 to 800 °C, there is another weight loss due to decomposition of SO_4^{2-}.[12] The TG curves of 2- and 2.5-nm nanocrystals rise from 100 to 200 °C and then from 220 to 960 °C for the former and from 220 to 960 °C for the latter, which results from the reaction between oxygen and the nanocrystals. Rapid elimination of chemically adsorbed *n*-octanol molecules will cause a small rise in the TG curves because of oxygen absorption by the denuded Co cations formerly coordinated with alcohol molecules.[8j] However, the calculated loss of 9.530×10^{-6} mol of adsorbed *n*-octanol molecules is small compared to the large increase of 4.3639×10^{-5} mol O in the TG curves. Thus, the weight increases are probably the result of oxygen replacing *n*-octanol and oxidation of surface Co(II) to Co(III) by oxygen. The sharp drops at ca. 950 °C are associated with the thermo-decomposition of Co_3O_4 ($Co_3O_4 = 3CoO + 1/2O_2\uparrow$).[8c]

The IR absorption peaks at ca. 664.61 and 578.05 cm^{-1} shown in Figure 3b confirm the formation of Co_3O_4 spinel oxide.[13] The broad bands centered at ca. 3400 cm^{-1} and the

---

(9) (a) Barr, T. L. *Modern ESCA*; Chemical Rubber: Boca Raton, FL, 1994. (b) Barr, T. L.; Seal, S. *J. Vac. Sci. Technol. A* **1995**, *13*, 1239. (c) Alexander, M. R.; Payan, S.; Duc, T. M. *Surf. Interface Anal.* **1998**, *26*, 961.

(10) Wang, Z. L.; Harfenist, S. A.; Vezmar, I.; Whetten, R. L.; Bentley, J.; Evans, N. D.; Alexander, K. B. *Adv. Mater.* **1998**, *10*, 808.

(11) Azarof, L. V.; Buerger, M. J. *The Powder Method in X-ray Crystallography*; McGraw-Hill: New York, 1958.

(12) (a) He, T.; Jiao, X.; Chen, D.; Lü, M.; Yuan, D.; Xu, D. *J. Non-Cryst. Solids* **1990**, *121*, 417. (b) Bokhimi, X.; Morales, A.; Portilla, M.; Lopez, T.; Tzomantzi, F.; Gomez, R. *J. Solid State Chem.* **1998**, *135*, 28.

(13) Gaddsden, J. A. *Infrared Spectra of Minerals and Related Inorganic Compounds*; Butterworth: London, 1975; p 44.

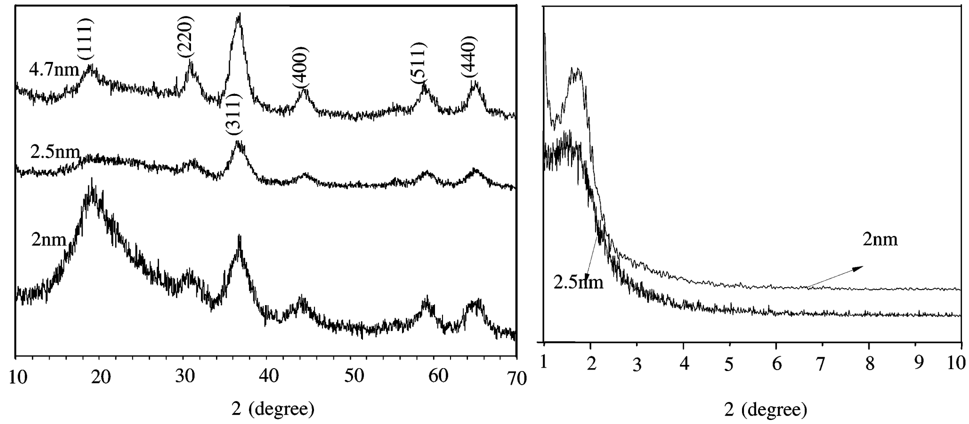

Figure 2. (a) XRD patterns of 2-, 2.5-, and 4.7-nm Co_3O_4 nanocrystals; (b) LAXRD patterns of 2- and 2.5-nm Co_3O_4 nanocrystals.

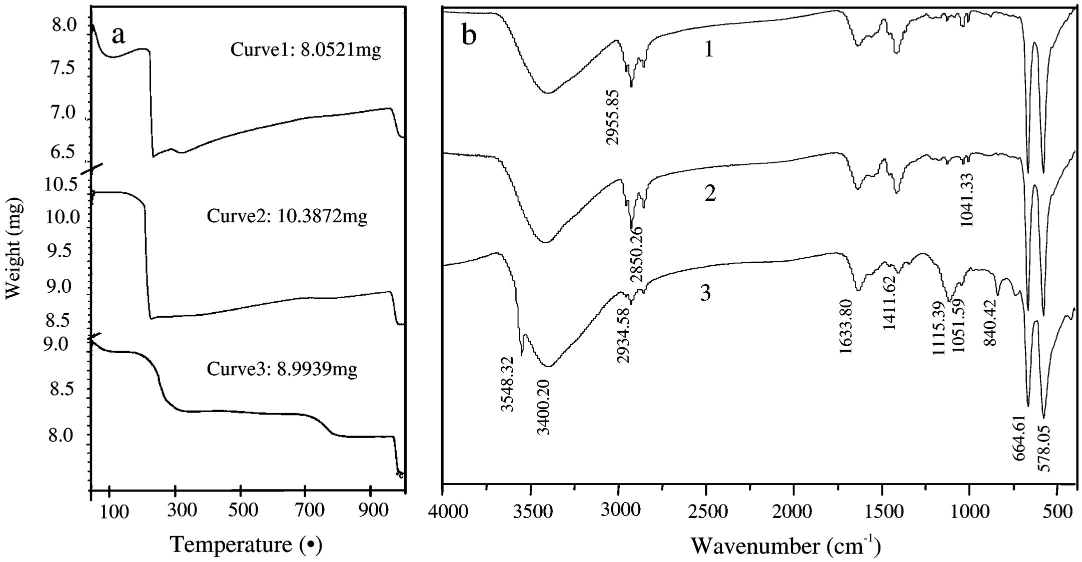

Figure 3. TG curves (a) and IR spectra (b) of 2- (1), 2.5- (2), and 4.7-nm (3) Co_3O_4 nanocrystals.

peaks at ca. 1633 cm^{-1} are assigned to the O−H stretching and bending modes of water.[14] The absorptions centered at 2900 cm^{-1} are assigned to C−H stretching vibrations. Although XPS analyses show that a small amount of sulfur (<1 mol %) exists on the nanocrystal surfaces, absorptions attributed to S−O vibrations in SDBS (ca. 1189 and 1131 cm^{-1})[15] were not detected. The absorption at ca. 1115 cm^{-1}, assigned to the asymmetric stretching mode of SO_4^{2-} anions, demonstrates the existence of SO_4^{2-} anions in the Co_3O_4 nanocrystals.[16] Thus, the hydrocarbons on the nanocrystals' surface are mainly *n*-octanol molecules. The absorptions corresponding to C−O stretching and C−H and O−H deformation modes in *n*-octanol are usually located at ca. 1050 and ∼1500−1400 cm^{-1} (see Supporting Information, Figure S2).[17] The weakening of C−O and O−H absorptions indicates a chemical interaction between the adsorbed *n*-octanol molecules and the Co ions on the nanocrystal surfaces. The sharp peak at 3548 cm^{-1} in Figure 3b3 indicates the existence of free hydroxyls.[18] The IR absorptions at ca. 1550 and 1415 cm^{-1} of the heated nanocrystals indicate the presence of trace carboxylate on the surface (Supporting Information, Figure S2).

XPS analysis indicates that sulfur (<1 mol %, corresponding to SO_4^{2-}) exists on the surface of Co_3O_4 nanocrystals, with molar contents of ca. 0.50% in 2- and 2.5-nm crystals and 0.75% in the 4.7-nm crystal sample. The bands at ∼799.9−780.0 eV (Co 2p $^3/_2$ binding energy), ∼795.1−795.2 eV (Co 2p $^1/_2$ binding energy), and ∼15.1−15.2 eV (spin−orbit splitting) are identical to those of pure Co_3O_4, and the shake-up satellites (I) with a low intensity at ca. 9 eV from the main spin−orbit components are also characteristic of those of pure Co_3O_4 (parts a−c of Figure 4).[19] The shake-up satellites (II) at ca. 5.6 eV from the Co 2p bands reveal the presence of surface hydroxyls (parts a−c

---

(14) Nakamoto, K. (Trans: Huang, D.; Wang, R.) *Infrared Spectra of inorganic and coordination compound*; 4th Chemical Industry Press: Beijing, 1991; p 251.

(15) Bellamy, L. J. (Trans: Huang, W.; Nie, C.) *Infrared Spectra of Complicated Molecules*; Science Press: Beijing, 1975; p 454.

(16) Wen, L. *The Infrared Spectroscopy of Minerals*; Chongqing University Press: Chongqing, China, 1988; p 61.

(17) Bellamy, L. J. (Trans: Huang, W.; Nie, C.) *Infrared Spectra of Complicated Molecules*; Science Press: Beijing, 1975; p107.

(18) (a) Bellamy, L. J. (Trans: Huang, W.; Nie, C.) *Infrared Spectra of Complicated Molecules*; Science Press: Beijing, 1975; p 212. (b) Arenas, J. F.; Marcos, J. I. *Spectrochim. Acta, Part A* **1979**, *35*, 355.

(19) (a) Castner, D. G.; Watson, P. R.; Chan, I. Y. *J. Phys. Chem.* **1989**, *93*, 3188. (b) Jiménez, V. M.; Fernández, A.; Espinós, J. P.; González-Elipe, A. R. *J. Electron Spectrosc. Relat. Phenom.* **1995**, *71*, 61. (c) Estrada, W.; Fantini, M. C. A.; de Castro, S. C.; Polo da Fonseca, C. N.; Gorenstein, A. *J. Appl. Phys.* **1993**, *74*, 5835. (d) Tyuliev, G.; Anglow, S. *Appl. Surf. Sci.* **1988**, *32*, 381.

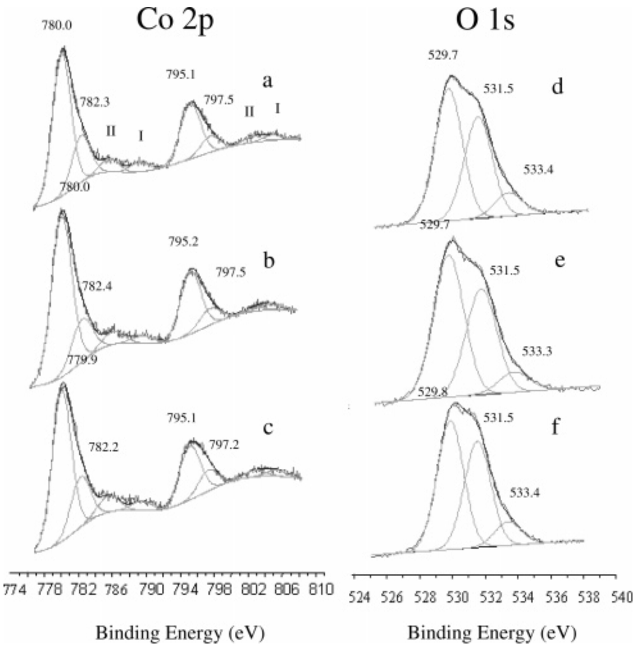

Figure 4. XPS analyses of Co 2p, O 1s for 2- (a and d), 2.5- (b and e), and 4.7-nm (d and f) Co_3O_4 nanocrystals.

of Figure 4).[20] The fact that their intensities increase along with the size of the nanocrystals indicates that the surface hydroxyl content increases along with particle size, which is consistent with the results of IR and TG analyses. The peaks at ~782.1−782.4 eV and ~797.2−797.5 eV result from a chemical shift of the main spin−orbit components because the Co cations on the nanocrystal surfaces chemically interact with *n*-octanol molecules, hydroxyls, and the trace carboxylate anions.[8d] The peaks at ~529.7−529.8, 531.5, and ~533.3−533.4 eV are assigned to oxygen species (O1s) in Co_3O_4, Co−OH/Co−HOC_8H_{17}, and H_2O molecules (Figure 4d, e, f).[8d]

3.3. Formation Mechanism of Co_3O_4 Nanocrystals. Since cobalt(II) nitrate is used as reagent, part of the Co(II) must be oxidized to give Co_3O_4 ($Co(II)Co(III)_2O_4$). Several experiments were carried out to study the process, and the results confirm a solubility-controlled mechanism for the redox reaction.

When the *n*-octanol solution as in experiments 1 or 2 was heated at 90 °C for 6 h, only $NaNO_3$ were detected by XRD in the precipitate, and the UV−vis spectrum showed SDBS, but no nitrate anions in the supernatant was present (Supporting Information, Figure S3), confirming that the metathesis reaction between $Co(NO_3)_2$ and SDBS occurs during the low-temperature reaction stage. Further experiments confirmed that sodium nitrate could be dissolved at 180 °C when water, DMSO, or methanol was added, for example, the solubility of sodium nitrate in a solution of 240 μL of deionized water/22 mL *n*-octanol is measured to be ca. 43 mg at 180 °C (Supporting Information, Figure S4).

In experiment 3 where water, DMSO, or methanol is absent, except for the precipitated sodium nitrate, no Co_3O_4 or other crystalline product forms after heat treatment at 180 °C for 6 h. The result in experiment 3 excludes the possibility that decomposition of the precipitated sodium nitrate produces necessary oxidants for oxidation of divalent cobalt ions. In contrast, Co_3O_4 forms when DMSO (experiment 4) or methanol (experiment 5) is added. It is reasonable to deduce that the dissolution of sodium nitrate in the system is critical for the formation of Co_3O_4 particles. As a common oxidant, nitrate anions can oxidize the Co(II) species in the system at high temperature.[8c] When the precipitated sodium nitrate is removed from the reaction system (experiment 6), no Co_3O_4 or other intermediate products are formed despite extended heat treatment at high temperature. All of the above evidence confirms that the redox process as well as the nucleation and growth of Co_3O_4 is controlled by the redissolving of the precipitated sodium nitrate.

Approximately 378 mg of the precipitated sodium nitrate in the typical experiment cannot be dissolved instantly, and the dissolution process actually stands in a dynamic equilibrium. The solubility of sodium nitrate could be adjusted by changing the quantity of water added. Therefore, the importance of the solubility-controlled process lies in generating a roughly constant reactant concentration during the reaction. Dissolved nitrate ions are generally consumed during the redox, which causes the precipitated sodium nitrate to dissolve further.

On the basis of the change of monomer concentration with reaction time, the formation of colloid particles is divided into 3 stages: monomer concentration increasing stage, nucleation stage, and growth stage.[21] The key to obtain monodispersed colloid particles lies in the separation of nucleation and growth, which has been achieved in the laboratory when the rapid-injection-based techniques are applied.[4] In the solubility-controlled process, rapid injection is replaced by dissolution, so the reaction rate at a certain temperature is only determined by the concentration of reactants, that is, by the solubility of sodium nitrate. Therefore, when the reaction rate is kept at a proper value, the monomer concentration after nucleation cannot reach the supersaturation for nucleation, so secondary nucleation is avoided. On the other hand, when both dissolution and redox reaction occur continuously, Co_3O_4 monomer is continually supplied and its concentration is always between the required concentration for nucleation and that for grain growth until the sodium nitrate is completely consumed. As a result, interparticle Ostwald ripening will not occur until all the sodium nitrate is consumed and uniform particles are obtained.[3]

The UV−vis spectra of Co_3O_4 nanocrystals (Figure 5a) exhibit two absorptions centered at ca. 400 and 680 nm, which are assigned to the ligand−metal charge transfers $O^{II} \rightarrow Co^{II}$ and $O^{II} \rightarrow Co^{III}$, respectively.[22] Compared with the absorptions at 480 and 760 nm of 47-nm nanocubes reported by Zeng et al.,[8d] the corresponding absorptions are blue-shifted by ca. 80 nm. The significant blue-shift is caused mainly by the quantum size effect of nanocrystals. UV−vis absorption spectra of the reaction liquids in the typical

---

(20) Mclntyre, N. S.; Cook, M. G. *Anal. Chem.* **1975**, *47*, 2208.

(21) LaMer, V. K.; Dinegar, R. H. *J. Am. Chem. Soc.* **1950**, *72*, 4847.

(22) (a) Cheng, C.-S.; Serizawa, M.; Sakata, H.; Hirayama, T. *Mater. Chem. Phys.* **1998**, *53*, 225. (b) Barreca, D.; Massignan, C.; Daolio, S.; Fabrizio, M.; Piccirillo, C.; Armelao, L.; Tondello, E. *Chem. Mater* **2001**, *13*, 588.

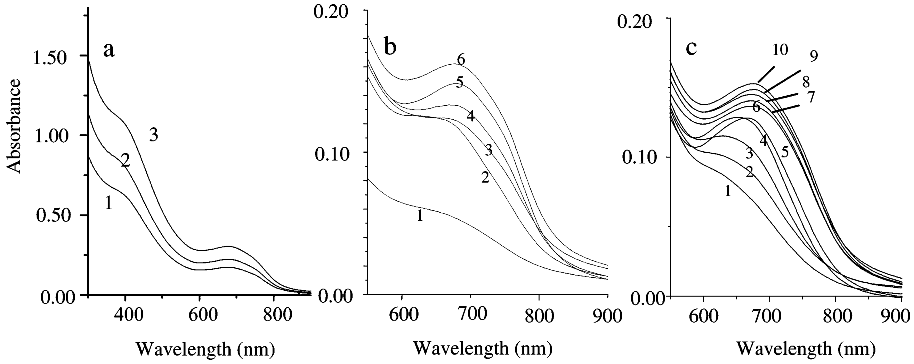

Figure 5. UV−vis absorption curves of (a1) 2-, (a2) 2.5-, and (a3) 4.7-nm Co_3O_4 nanocrystals and the reaction liquids at 180 °C for (b1) 20 min, (b2) 40 min, (b3) 60 min, (b4) 90 min, (b5) 120 min, (b6) 150 min and at 160 °C for (c1) 20 min, (c2) 40 min, (c3) 60 min, (c4) 80 min, (c5) 100 min, (c6) 120 min, (c7) 150 min, (c8) 180 min, (c9) 210 min, (c10) 240 min. (The as-prepared Co_3O_4 nanocrystals as well as a same volume of the reaction liquids (0.5 mL) obtained after different reaction times were dissolved into ca. 10 mL of cyclohexane to form transparent solutions. Cyclohexane was used as the blank. There are no absorptions for SDBS and nitrate anions in the range of 300∼900 nm).

synthesis experiment for different reaction durations are shown in Figure 5b. The absorbance of the band from 500 to 900 nm increases with time, and at the same time, the center of the absorption peaks shows a progressive red-shift. Moreover, the magnitude of the red shift from b2 to b6 (∼40−150 min) decreases gradually. For example, the absorption peak is red shifted ca. 13 nm when the reaction duration is increased by 20 min, from b2 to b3 (∼40−60 min). In contrast, a red-shift of only ca. 2 nm occurs between 60 and 150 min (b3 to b6). The evolution of the absorption curves over time shows the separation of nucleation and growth in the solubility-controlled synthetic process. The fact that the absorbance increases from b1 to b2 indicates that more Co^{III}−O octahedrons begin to form and, similarly, the absorbance of the peak assigned to $O^{II} \rightarrow Co^{II}$ ligand−metal charge transfers also increases at this time, indicating the formation of more Co^{II}−O tetrahedrons (Supporting Information, Figure S5). In a unit cell of spinel oxide Co_3O_4, two Co^{III} cations exist in the center of oxygen octahedra and one Co^{II} cation is in the center of an oxygen tetrahedron.[23] The curves' evolution at this point thus could be attributed to the formation of Co_3O_4 monomers (maybe larger molecules or clusters). The red-shift of absorption from b2 to b6 indicates growth of nanocrystal, and the relatively larger magnitude of the red-shift from b2 to b3 denotes a much larger growth rate, which is consistent with a previous report.[3]

The absorption curve evolution from b1 to b2 reflects the nucleation process, and curve b2 could be roughly regarded as the burst-nucleation point.[21] At that point, the great mass of accumulated monomers are quickly consumed due to rapid formation of a large number of nuclei. As a result, monomer concentration decreases quickly into the growth range in LaMer's curve and the separation of nucleation and growth is achieved.[21] Because of the small solubility of sodium nitrate, the limited number of monomers formed per unit time does not allow the concentration to enter the nucleation range again but instead ensures a slow growth rate. Thus, the solubility-controlled redox process separates nucleation and growth.

When excess water or DMSO is added, polydispersed Co_3O_4 nanocubes are obtained. In this case, more Co_3O_4 monomers are formed per unit time than those consumed by growth because of the excessively large solubility of sodium nitrate, and the monomer concentration is boosted back into the nucleation range; consequently, the secondary nucleation occurs causing a broad particle size distribution.

The nucleation and growth of nanocrystals at different temperatures were also tracked with UV−visible spectroscopy. The absorption changes are similar to those in the typical synthesis. Figure 5c gives absorption curves over time at 160 °C. The lower reaction temperature decreases the rate of both the redox reaction and the growth of the nanocrystals. Curves c1−c4 correspond to the nucleation stage, and curves c4−c10 correspond to the growth stage of the nanocrystals. Curve c4 is roughly regarded as the burst-nucleation point.

When the reaction time is prolonged, interparticle Ostwald ripening[3] occurs in the synthetic process. On the basis of Lifshitz, Slyozov, and Wagner's theory,[24] a detailed mathematical description of Ostwald ripening theory, the particle size is proportional to the cube root of time for a diffusion controlled process. The variation of cube size versus reaction time are shown in Figure 6a, obviously there is no direct proportion between the two parameters. Although the cube-like morphology of the products contrasts with the theory's assumption of a spherical crystallite, it also indicates that the increase of the nanocrystal sizes over a long period of time is not dominated by interparticle coarsening. Coarsening growth usually causes defocusing of the particle size distribution, while in solubility-controlled synthetic process the nanocrystals always grow with a narrow particle size distribution over long periods of time (for example, 3 h at 180 °C or 4 h at 160 °C). When the reaction is carried out for much longer times (for example, at 140 °C for 72 h) so that all the sodium nitrate is consumed, interparticle coarsening takes place since the solubility-controlled mechanism is no longer controlling the growth. The TEM image in Figure 6b demonstrates that the average particle size is ca. 10 nm and that the particle size distribution is markedly broadened. The particle sizes of some nanocrystals are smaller than 5 nm, and their shape becomes more spherical due to dissolving. Most of the nanocubes are imperfect, because of

---

(23) Smith, W. L.; Hobson, A. D. *Acta Crystallogr. B* **1973**, *29*, 362.

(24) (a) Lifshitz, I. M.; Slyozov, V. V. *J. Phys. Chem. Solids* **1961**, *19*, 35. (b) Wagner, C. *Z. Elektro-chem.* **1961**, *65*, 581.

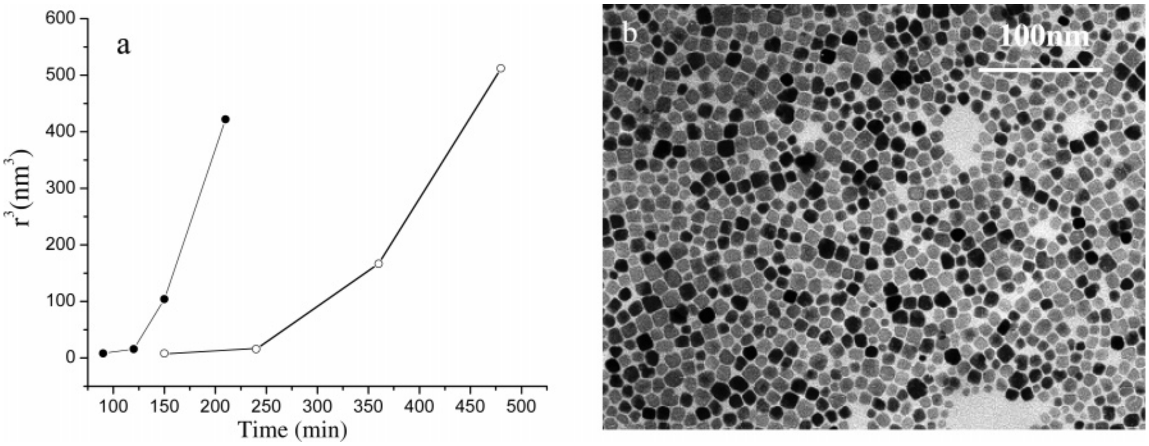

Figure 6. (a) The variations of the cube of particle size vs the reaction time (reaction temperature: ●, 180 °C; ○, 160 °C). (b) TEM images of Co_3O_4 nanocrystals obtained when the reaction is carried out at 140 °C for 72 h.

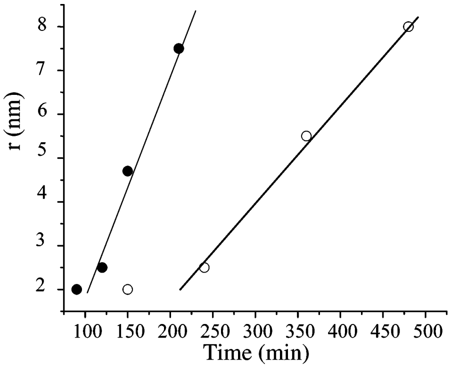

Figure 7. The variations of the particle size vs the reaction time (reaction temperature: ●, 180 °C; ○, 160 °C).

preferential dissolving since atoms at the edges and apex have relatively high chemical potentials.

In the solubility-controlled process, constant reactant concentration results in the redox reaction occurring at a constant rate. Since no secondary nucleation or coarsening growth occurs when the solubility-controlled mechanism dominates, the growth rate of the nanocrystals is roughly equal to the redox reaction rate, that is, the number of Co_3O_4 monomers consumed per unit time due to the growth of nanocrystal is equal to that of the Co_3O_4 monomers produced by the solubility-controlled redox reaction. Consequently, the following equation can be drawn. At a certain reaction temperature, $\nu M/3\rho r_0^2$ is a constant. Therefore, it is concluded that during the solubility-controlled growth the size of the cubelike nanocrystals r is linear with the reaction time t, which is roughly consistent with the experiment results (Figure 7)

$$(\rho\, dV)/M = \nu\, dt$$

$$\rho[(r_0 + dr)^3 - r_0^3]/M = \nu dt$$

$$\rho(r_0^3 + 3r_0^2\, dr + 3r_0\, dr^2 + dr^3 - r_0^3)/M = \nu\, dt$$

$$3\rho r_0^2\, dr/M = \nu\, dt$$

$$dr = (\nu M/3\rho r_0^2)\, dt$$

where ρ is the density of Co_3O_4, V the volume of the Co_3O_4 nanocrystals, M the molecular weight of Co_3O_4, ν the reaction rate of the redox reaction, t the reaction time, and r_0 the size of the nanocrystal on a side at t_0 moment.

Table 2. Change of Co_3O_4 Nanocrystal Size and Shape with Reaction Time and Temperature

reaction temperature/time	particle size	particle shape
180 °C/1.5 h	2 nm	spherelike
180 °C/2 h	2.5 nm	cubelike
160 °C/2.5 h	2 nm	spherelike
160 °C/4 h	2.5 nm	cubelike

Recently, syntheses of nanocrystals with cubelike shapes, whose crystallographic symmetry belongs to the cubic system, have been intensively investigated.[8c,25] A low growth rate usually controlled by a low monomer concentration is critical for nanocube formation, in which the thermodynamic factors play an important role in shape control.[25c] When the particle size reaches the nanometer scale, the effect of surface energy on crystal growth becomes more and more important. The {100} planes of spinel oxides, which have cubic crystallographic symmetry, are predicted to have the lowest surface energy.[26] The growth of spinel nanocrystals tends to be terminated at their {100} planes under thermodynamic control. As a result, the nanocrystals have cubelike shapes.[25c] In the solubility-controlled synthetic process, the growth rate is slow since the monomer concentration is limited. Therefore, the formation of Co_3O_4 nanocubes is attributed to shape control by thermodynamic factors. The shape evolution of nanocrystals over reaction duration confirms that the smallest particle size for Co_3O_4 crystallites with a cubelike shape is 2.5 nm (see Table 2). Furthermore, a few 2.5-nm nanocubes were also detected in HRTEM images of 2-nm nanospheres, which confirms that the nanocubes are formed from nanospheres when their size reaches 2.5 nm (Supporting Information, Figure S6). Most of the atoms are on the nanocrystals' surface when the particle size is not larger than 2 nm. And

---

(25) (a) Yu, D.; Yam, V. W. W. *J. Am. Chem. Soc.* **2004**, *126*, 13200. (b) Kim, F.; Connor, S.; Song, H.; Kuykendall, T.; Yang, P. *Angew. Chem., Int. Ed.* **2004**, *43*, 3673. (c) Song, Q.; Zhang, Z. J. *J. Am. Chem. Soc.* **2004**, *126*, 6164. (d) Xia, Y.; Sun, Y. *Science* **2002**, *298*, 2176. (e) Lee, S. M.; Jun, Y. W.; Cho, S. N.; Cheon, J. *J. Am. Chem. Soc.* **2002**, *124*, 11244. (f) Dumestre, F.; Chaudret, B.; Amiens, C.; Renaud, P.; Fejes, P. *Science* **2004**, *303*, 821. (g) Agnoli, F.; Zhou, W.; O'Connor, C. J. *Adv. Mater.* **2001**, *13*, 1697. (h) Jun, Y. W.; Jung, Y. Y.; Cheon, J. *J. Am. Chem. Soc.* **2002**, *124*, 615. (i) Ahmadi, T. S.; Wang, Z. L.; Henglein, A.; El-Sayed, M. A. *Chem. Mater.* **1996**, *8*, 1161.

(26) (a) Davies, M. J.; Parker, S. C.; Watson, G. W. *J. Mater. Chem.* **1994**, *4*, 813. (b) Fang, C. M.; Parker, S. C.; De With, G. *J. Am. Ceram. Soc.* **2000**, *83*, 2082.

in order to minimize their surface energy, the crystallites usually exhibit a spherelike shape. Therefore, the appearance of critical size during the shape evolution demonstrates that the shapes of nanocrystals are mainly determined by thermodynamic factors in the solubility-controlled synthesis. As a counterexample, Co_3O_4 nanocrystals capped with long-carbon chain alcohol molecules have been prepared by a rapid-injection method, but the fast growth under much higher monomer concentration produces nanocrystals with an irregular flakelike shape.[8j]

4. Conclusions

Through a solubility-controlled liquid-phase reaction process, the controlled syntheses of monodispersed 2-nm (spherical), 2.5-nm (cubelike), and 4.7-nm (cubelike) Co_3O_4 nanocrystals have been achieved. In most liquid-phase precipitation processes, the separation of nucleation and growth is critical to obtain uniform particle size and shape. The solubility-controlled process exhibits a new concept where the thermodynamic and kinetics of a chemical reaction as well as the nucleation and growth of nanocrystals are controlled by changing reactants' solubility. Not only has separation of nucleation and growth been achieved but most importantly the nucleation and growth occurred at a controlled and constant monomer concentration, making the control over particle size feasible.

Supporting Information Available: TEM images of the 2-nm nanocrystals, IR spectra *n*-octanol and the 2-nm crystals, UV−vis spectra of SDBS, the supernatant, the dissolved sodium nitrate, and the reaction liquid, and HRTEM images of the 2-nm nanocrystals. This material is available free of charge via the Internet at http://pubs.acs.org.

CM050727S